Research Square

Preprints are preliminary reports that have not undergone peer review.
They should not be considered conclusive, used to inform clinical practice,
or referenced by the media as validated information.

Orbital Angular Momentum Carried by ShGB Vortex Beam for FSO and its Aberration Effects

Nimmy Lazer (nimmylazer.mcet@gmail.com)
Marthandam College of Engineering & Technology
Y. P. Arul Teen
University College of Engineering
K. B. Rajesh
Chikkanna Government Arts College

Research Article

Keywords: Vortex Sinh beam, z-tilt aberration, Defocus aberration, Astigmatism aberration, Coma aberration, Spherical aberration, Topological charge

Posted Date: April 6th, 2022

DOI: https://doi.org/10.21203/rs.3.rs-1512547/v1

License: This work is licensed under a Creative Commons Attribution 4.0 International License.
Read Full License

Orbital Angular Momentum Carried by ShGB Vortex Beam for FSO and its Aberration Effects

Nimmy Lazer[1*], Y. P. Arul Teen[2] and K. B. Rajesh[3]
[1]Department of ECE, Marthandam College of Engineering & Technology,
Marthandam, Tamilnadu 629177, India.
[2]Department of ECE, University College of Engineering,
Nagercoil, Tamilnadu 629004, India.
[3]Department of Physics, Chikkanna Government Arts College,
Tirupur, Tamilnadu 641602, India.
***Corresponding author mail: nimmylazer.mcet@gmail.com**

Abstract: In this paper, orbital angular momentum (OAM) and distribution of intensity of vortex Sinh-Gaussian beam (ShGB) travelling through an atmosphere with turbulence are detailly studied by applying Fresnel-Kirchhoff diffraction integral equations. When the medium of propagation of an optical beam in the atmosphere, it encounters so many issues. One of the main issues is atmospheric turbulence. A turbulent atmosphere is composed of various types of aberrations. Here, we have undergone a detailed investigation of the effect of various aberrations present in the atmosphere, such as z-tilt aberration, defocus aberration, astigmatism aberration, coma aberration, and spherical aberration under zero, weak, medium, and strong turbulent conditions. Also, it noted its OAM and the distribution of intensity of the vortex ShGB with topological charge p=1 at different propagation distances (z=2000m & z=5000m) under a turbulent atmosphere. Numerical analysis results of each aberration show that all aberrations have some sort of impact on vortex ShGB. But on comparing the results of all aberrations, it is observed that the consequence of tilt aberration is greater than the other four aberrations on vortex ShGB. From the simulation results, it is found that the beam gets converted into a Gaussian nature when the value of turbulence factor is increased from zero turbulent condition to strong turbulent condition. Therefore, the resultant OAM and intensity distribution of vortex ShGB due to the effect of z-tilt aberration contribute a crucial part when compared with the other four aberrations. Also, it is noticed that the beam is least affected by coma aberration. The results also show that as we increase the distance of propagation from 2000m to 5000m, the quality of the beam gets reduced.
Keywords: Vortex Sinh beam; z-tilt aberration; Defocus aberration; Astigmatism aberration; Coma aberration; Spherical aberration; Topological charge.

1. INTRODUCTION

Recently, a growing interest has been exhibited in the analysis of spectral behaviour of various Gaussian beams in turbulent atmospheres. A turbulent atmosphere consists of numerous aberrations such as z-tilt, defocus, astigmatism, coma, and spherical aberration. The impact of tilt and astigmatism aberration on a vortex carrying Gaussian beam was analysed detailly earlier in [1]. The outcomes showed that the aberration named tilt conquers severe influence on the quality of the beam. The influence on BG beam due to aberrations such as tilt as well as astigmatism aberration was analysed, and it was proved that a major defect is caused because

of tilt aberration by Arul et al. [2]. The distribution of intensity of vortex beams without and with aberration is being investigated [3,4]. Wang et al. [5,6], in their paper, proved spreading of the beam is less affected in vortex beams than in non-vortex beams when it propagates through the turbulent atmosphere. The longitudinally polarised focusing performance of ShGB was analysed by Jie et al. [7]. The tight centring nature of an azimuthally polarised ShGB, modulating its phase with a multi-belt vortex phase filter applying vector diffraction theory, was investigated in [8]. Under turbulent atmosphere, aperture scintillation effects and the average bit error rate of ShGB was detailly analysed in [9]. Propagation properties and optical forces of the Hollow Sinh Gaussian (HsG) beam was performed on a Rayleigh dielectric sphere in [10]. As the propagation distances increase, the OAM decreases from the optical axis to the vortex centres [11]. Also, HsGB can steadily propagate in strongly nonlocal nonlinear media [12]. Compared to other Gaussian beams, the most interesting features of HsGB mainly includes a much higher intensity gradient, enhanced trapping efficiency, significantly sharp, peak-centred, and adjustable intensity distribution. These features were clearly investigated in [13].

In this paper, to identify the role of aberrations in maintaining the beam quality, we have studied the performance of vortex ShGB in the presence of several aberrations such as z-tilt, defocus, astigmatism, coma, and spherical aberration. Also, OAM and distribution of intensity of vortex ShGB are judged by applying Fresnel-Kirchhoff diffraction integral for p=1 topological charge at two values of propagation distances under four different structural constants of atmosphere. A small description of OAM is described in section 2. A brief theoretical description of the vortex ShGB beam is mentioned in section 3. The influence of aberrations present in a turbulent atmosphere on ShGB's distribution of intensity is clearly mentioned in the 4th section. In the 5th section, the results based on numerical calculations of various aberrations during the propagation of the beam through the channel having z-tilt, defocus, astigmatism, coma, and spherical aberration are shown. In section 6, a comparison between each aberration at different propagation distances (z=2000m & z=5000m) is provided, and the conclusion is presented in section 7.

2. ORBITAL ANGULAR MOMENTUM (OAM)

A very dominant property that exists in light is known as the phase vortex. The beam waist of a Gaussian beam has a planar wavefront (phase front) [14]. A wavefront can be defined as the locus of points on a 3D surface that can be noted during its propagation by monitoring the position with respect to the same spatial phase. A beam of light with a wavefront in the form of a spiral is known as the phase vortex. A phase vortex with a spiral wavefront occupies OAM. All the light beams with phase vortex consist of a phase term $exp(ip\epsilon)$, which has an OAM of ith per photon with topological charge p and an azimuthal angle ϵ. Light beams that depend on the spatial distribution of the field acquires OAM. Angular momentum of a light beam, which produces a helical or twisted wavefront, is due to the existence of internal OAM, which is independent of origin. The external OAM is dependent on origin. Calculation of angular momentum can be done by taking the cross product of the optical beam's position and its overall linear momentum. Vortex ShGB beams are very much focused due to their inherent characteristics. The radius of the dark spot surrounded by the ring of the beam is controlled by the beam order, and it can maintain the mode profile for long-distance propagation. The

phenomenon of restricting the vibrations into a particular plane is known as polarisation. Light beams commonly belong to either radially polarised beam (TM_{01}) or azimuthally polarised beam (TE_{01}). These are the most common cylindrical vector beams. A beam of light is said to be radially polarised if the polarisation vector at every position of the beam point towards the middle of the beam. In an azimuthally polarised beam of light, the polarisation vector is tangential to the beam. Fig. 1(a & b) shows the radially and azimuthally polarised beam along with OAM values +1 and -1. The intensity distribution of doughnut-shaped can be clearly seen in Fig. 1(c) and 1(d).

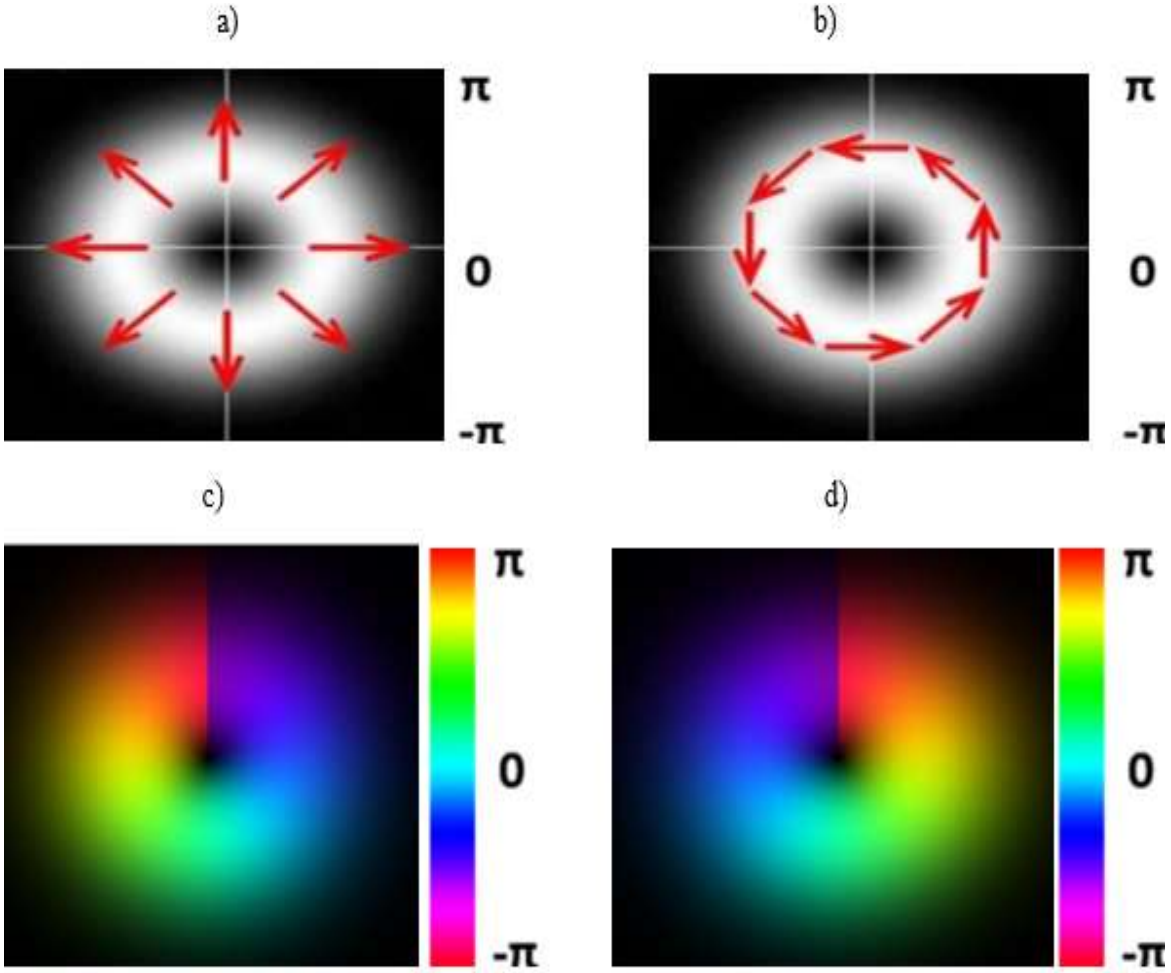

Fig. 1 Simple demonstration of field distributions (a) Radially polarised beam (TM_{01}) (b) Azimuthally polarised beam (TE_{01}). (c) OAM with p=+1 topological charge. (d) OAM with =-1 topological charge

A beam that carries an optical vortex is known as OAM [15]. Some of the distinctive features of optical vortex include processing of optical information, photonic computer, optical communication, and so on. Since the dimension of OAM varies with change in the value of amplitude, phase, frequency, and polarisation, vortex beam can carry unlimited orthogonal OAM states. This leads to an increased number of channels and a larger capacity of the channel. OAM technology can be implemented by combing wavelength division multiplexing, pulse density modulation, etc. A vortex ShGB beam can be generated with the help of a spatial light modulator (SLM) from a non-vortex HsG beam, as shown in Fig. 2.

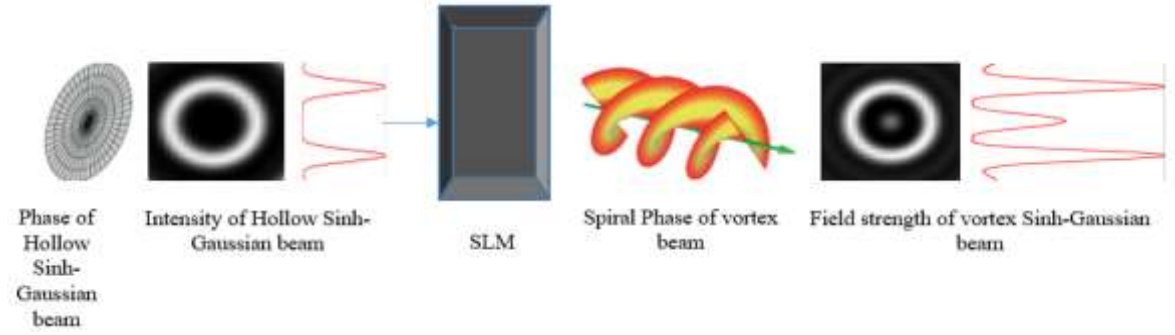

Fig. 2 Obtaining vortex Sinh-Gaussian beam from Hollow Sinh-Gaussian beam using SLM

3.THEORY

The fundamental property of optical vortex is the phase profile, and it is given by the equation,

$$\varphi(r, \epsilon, z) = p\epsilon \tag{1}$$

where (r, ϵ, z) are the cylindrical polar coordinates, the path of the vortex core is z, ϵ is the azimuthal coordinate on the z =0 plane, and p is the topological charge. The electric field of a single vortex beam is,

$$U_n(r, \epsilon, z = 0) = A_m(r, z = 0)\, exp(ip\epsilon) \tag{2}$$

Where A_m is a radially symmetric amplitude profile function, the radiating electromagnetic field can be described with the help of a topological charge. Now the equation of an optical beam travelling towards z-direction with a single vortex at r=0 is,

$$U_n(r, \epsilon, z = 0) = A_m(r, z = 0)exp(ip\epsilon)exp(i\varphi_m(r, z)) \tag{3}$$

where φ_m is the phase.

The electric field of Sinh-Gaussian beam without vortex as per [10,16-18] can be written as,

$$E_n(r, 0) = G_0 sinh^n\left(\frac{b}{w}\right) exp\left(-\frac{b^2}{w^2}\right) \tag{4}$$

where, G_0 is a constant related beam power P_0, w is the focus of the optical beam, beam radius is b, n=0,1,2,…is the order of beam. We can convert an HsG beam into a vortex ShGB beam by including the vortex component, and its equation for the electric field can be written as,

$$E_n(r, 0) = G_0 sinh^n(\gamma) exp(-\gamma^2) exp(ip\epsilon) \tag{5}$$

where p is the topological charge, $\exp(ip\epsilon)$ is the vortex term and $\gamma = \frac{b}{w}$ is a truncation parameter with beam focus w.

The phasor of vortex ShGB beam can be written as,

$$E(\rho, \epsilon, z = 0) = E_0 E_n(r, 0) \tag{6}$$

where, E_0 is the characteristic magnitude, ρ is the geometrical distance of a point generating from its centre its radius b, the azimuthal coordinate is ϵ, and z is the propagation distance. By substituting Eq. (5) in Eq. (6), we get,

$$E(\rho, \epsilon, z = 0) = E_0 G_0 sinh^n(\gamma\rho) exp(-\gamma^2\rho^2) exp(ip\epsilon) \tag{7}$$

By the application of Fresnel–Kirchhoff diffraction integral with beam radius b, lens radius r, $\gamma = \frac{b}{w} = 1$, and $E_0 = 1$, the complex phasor of the observed plane is,

$$E(r,\varphi,z) \quad = C_1 \int_0^1 \int_0^{2\pi} E(\rho,\epsilon,z=0) exp\{iS(\rho,\epsilon)\} \times exp\left[-i\frac{2\pi b}{\lambda z} r\rho\, cos(\epsilon - \emptyset)\right] \rho d\rho d\epsilon \quad (8)$$

where $C_1 = a^2 exp\frac{(kz+i\pi r^2/\lambda z)}{i\lambda z}$ and $S(r,\epsilon) = a_1 + S_{tilt} + S_{defo} + S_{asti} + S_{coma} + S_{sphe}$ *i*s the overall aberration in a turbulent atmosphere, a_1 is a constant, and the expression for S_{tilt} aberration is, $S_{tilt}(\chi) = 2a_2 r cos\epsilon + 2a_3 r sin2\epsilon$,the defocus S_{defo} is given by $S_{defo}(\rho,\epsilon) = \sqrt{3}a_4^2\rho^2$, equation for astigmatism aberration is, $S_{asti}(\chi) = \sqrt{6}\,(a_5\rho^2 cos2\epsilon + a_6\rho^2 sin2\epsilon)$, the coma aberration is given by, $S_{coma}(\rho,\epsilon) = \sqrt{8}\langle a_{\{7,8\}}^2\rangle[\rho_1^8 + \rho_2^8 - 2\rho_1^3\rho_2^3 cos(3\epsilon_1 - 3\epsilon_2)]$, and the spherical aberration is given by $S_{sphe}(\rho,\epsilon) = \sqrt{10}(a_{11}\rho^4 cos4\epsilon + a_{11}\rho^4 sin4\epsilon)$[20,21].

4.EFFECTS OF VARIOUS ABERRATIONS ON THE INTENSITY DISTRIBUTION OF BEAMS

4.1 Z-tilt aberration

The function for phase fluctuation due to z-tilt aberration in atmospheric turbulence is [3]

$$S_{tilt}(\rho,\epsilon) = 2a_2\rho cos\epsilon + 2a_3\rho sin\epsilon \quad (9)$$

here, a_2 and a_3 are the second and third-order of Zernike coefficients. The phasor of observation plane under tilt aberration is,

$$U_n(r,\varphi,z) = C_1 \int_0^1 \int_0^{2\pi} sinh^n(\gamma\rho)\, exp(-\gamma^2\rho^2)\, exp(ip\epsilon)$$
$$exp[iS_{tilt}(\rho,\epsilon)]\, exp(-i\frac{2\pi b}{\lambda z} r\rho cos(\epsilon - \emptyset)\rho d\rho d\epsilon \quad (10)$$

The distribution of intensity of ShGB at z=0 is,

$$I(r,\varphi,z) = \langle |U_n(r,\varphi,z)|^2 \rangle \quad (11)$$

where ensemble average of turbulent factor is denoted using the notation $\langle . \rangle$. $I(r,\varphi,z)$ of the vortex, ShGB is obtained by substituting Eqn. (10) in Eqn. (11) and after making some arrangements, it can be written as,

$$I(r,\varphi,z) = C_1 \int_0^1 \int_0^{2\pi} \int_0^1 \int_0^{2\pi} sinh^{2n}(\gamma(\rho_1 + \rho_2)\, exp(-\gamma^2({\rho_1}^2 + {\rho_2}^2))\, exp\big(ip(\epsilon_1 - \epsilon_2)\big)\, exp\left\{-\frac{1}{2} D_{tilt}\big(\rho_1,\rho_2,\epsilon_1,\epsilon_2\big)\right\} exp(i\pi\left(\frac{2b}{\lambda z}\right) r[\rho_2\, cos(\epsilon_2 - \emptyset) - \rho_1 cos(\epsilon_1 - \emptyset)]]\rho_1\rho_2 d\rho_1 d\epsilon_1 d\rho_2 d\epsilon_2 \quad (12)$$

here, $D_{tilt}(\overrightarrow{\rho_1},\overrightarrow{\rho_2})$ is the wave function, and the variance for tilt is,

$$D_{tilt}(\rho,\epsilon) = 4\langle a_{\{2,3\}}^2\rangle[\rho_1^2 + \rho_2^2 - 2\rho_1\rho_2 cos(\epsilon_1 - \epsilon_2)] \quad (13)$$

$$\text{where, } \langle a_{\{2,3\}}^2\rangle = 0.448(\frac{D}{r_0})^{\frac{5}{3}} \quad (14)$$

where the diameter of the aperture is D, Fried's coherence length is $r_0=(0.432k^2{C_n}^2z)^{-3/5}$, the atmospheric structural constant is ${C_n}^2$, and the turbulence layer thickness and distance of propagation is z. Substituting Eqns. (13) and (14) in (12) we get [19-20],

$$I(r,\varphi,z) = C_1 \int_0^1 \int_0^{2\pi} \int_0^1 \int_0^{2\pi} sinh^{2n}(\gamma(\rho_1+\rho_2)\, exp(-\gamma^2(\rho_1^2+\rho_2^2))\, exp(ip(\epsilon_1 - \epsilon_2)) \times exp\left\{-0.387 D^{5/3} k^2 C_n^2 z(\rho_1^2+\rho_2^2-2\rho_1\rho_2 cos(\epsilon_1-\epsilon_2))\right\} exp\left[i\pi\left(\frac{2b}{\lambda z}\right) r[\rho_2\, cos(\epsilon_2 - \emptyset) - \rho_1 cos(\epsilon_1 - \emptyset)]\right] \rho_1\rho_2 d\rho_1 d\epsilon_1 d\rho_2 d\epsilon_2 \quad (15)$$

4.2 Defocus aberration

The expression for defocus phase aberration is given by,

$$S_{defo}(\rho,\epsilon) = \sqrt{3} a_4^2 \rho^2 \quad (16)$$

where a_4 is the 4th coefficient of Zernike polynomials. I(r, φ, z) on the ShGB is,

$$I(r,\varphi,z) = C_1 \int_0^1 \int_0^{2\pi} \int_0^1 \int_0^{2\pi} sinh^{2n}(\gamma(\rho_1+\rho_2)\, exp(-\gamma^2({\rho_1}^2+{\rho_2}^2))\, exp\big(ip(\epsilon_1 - \epsilon_2)\big)\, exp\left\{-0.0149 D^{5/3} k^2 C_n^2 z(\rho_1^4+\rho_2^4-2\rho_1^2\rho_2^2\, cos(\epsilon_1-\epsilon_2))\right\} exp(i\pi\left(\frac{2b}{\lambda z}\right) r[\rho_2\, cos(\epsilon_2 - \emptyset) - \rho_1 cos(\epsilon_1 - \emptyset)]]\rho_1\rho_2 d\rho_1 d\epsilon_1 d\rho_2 d\epsilon_2 \quad (17)$$

4.3 Astigmatism aberration

The expression for astigmatism aberration is,

$$S_{asti}(\rho,\epsilon) = \sqrt{6\,}(a_5\rho^2 cos2\epsilon + a_6\rho^2 sin2\epsilon) \quad (18)$$

where a_5 and a_6 are the fifth and sixth-order Zernike polynomial coefficients, and the equation for astigmatism is,

$$D_{asti}(\rho,\epsilon) = \sqrt{6}\langle a_{\{5,6\}}^2\rangle[\rho_1^4+\rho_2^4-2\rho_1^2\rho_2^2 cos(2\epsilon_1-2\epsilon_2)] \quad (19)$$

here,

$$\langle a_{\{5,6\}}^2\rangle = 0.023\left(\frac{D}{r_0}\right)^{\frac{5}{3}} \quad (20)$$

Now I(r, φ, z) on the vortex ShGB is obtained by substituting Eqn. (19) into Eqn. (12),

$$I(r,\varphi,z) = C_1 \int_0^1 \int_0^{2\pi} \int_0^1 \int_0^{2\pi} sinh^{2n}(\gamma(\rho_1+\rho_2)\, exp(-\gamma^2(\rho_1^2+\rho_2^2))\, exp(ip(\epsilon_1 - \epsilon_2)) \times exp\left\{-0.0299 D^{5/3} k^2 C_n^2 z(\rho_1^4+\rho_2^4-2\rho_1^2\rho_2^2 cos(2\theta_1 - 2\theta_2))\right\} exp\left[i\pi\left(\frac{2b}{\lambda z}\right) r[\rho_2\, cos(\epsilon_2 - \emptyset) - \rho_1 cos(\epsilon_1 - \emptyset)]\right] \rho_1\rho_2 d\rho_1 d\epsilon_1 d\rho_2 d\epsilon_2 \quad (21)$$

4.4 Coma aberration

The expression for coma aberration is given by,

$$S_{coma}(\rho,\epsilon) = \sqrt{8}\langle a_{\{7,8\}}^2\rangle[\rho_1^8+\rho_2^8-2\rho_1^3\rho_2^3 cos(3\epsilon_1-3\epsilon_2)] \quad (22)$$

where a_7 and a_8 denote the seventh and eighth power of Zernike polynomials coefficients. Now the expression for coma aberration is,

$$D_{coma}(\rho,\epsilon) = \sqrt{8}\langle a_{\{7,8\}}^2\rangle[\rho_1^8+\rho_2^8-2\rho_1^3\rho_2^3 cos(3\epsilon_1-3\epsilon_2)] \quad (23)$$

Now I(r, φ, z) on the vortex ShGB is obtained by substituting Eqn. (23) into Eqn. (12),

$$I(r,\varphi,z) = C_1 \int_0^1 \int_0^{2\pi} \int_0^1 \int_0^{2\pi} sinh^{2n}(\gamma(\rho_1+\rho_2)\, exp\big(-\gamma^2(\rho_1^2+\rho_2^2)\big)\, exp(ip(\epsilon_1 - \epsilon_2)) \times exp\left\{-0.011 D^{5/3} k^2 C_n^2 z(\rho_1^8+\rho_2^8-2\rho_1^3\rho_2^3\, cos(3\epsilon_1 - 3\epsilon_2))\right\} exp\left[i\pi\left(\frac{2b}{\lambda z}\right) r[\rho_2\, cos(\epsilon_2 - \emptyset) - \rho_1\, cos(\epsilon_1 - \emptyset)]\right] \rho_1\rho_2 d\rho_1 d\epsilon_1 d\rho_2 d\epsilon_2 \quad (24)$$

4.5 Effects of spherical aberration

The expression for spherical aberration is given by,

$$S_{sphe}(\rho,\epsilon) = \sqrt{10}(a_{11}\rho^4 cos4\epsilon + a_{11}\rho^4 sin4\epsilon) \quad (25)$$

where a_{11} is the Zernike polynomials coefficient and expression for spherical aberration is,

$$D_{sphe}(\rho,\epsilon) = \sqrt{10}\langle a_{\{11\}}^2\rangle[\rho_1^{16} + \rho_2^{16} - 2\rho_1^4\rho_2^4 cos(4\epsilon_1 - 4\epsilon_2)] \quad (26)$$

Now I(r, φ, z) on the vortex ShGB can be obtained by substituting Eqn. (26) into Eqn. (12),

$$I(r,\varphi,z) = C_1 \int_0^1 \int_0^{2\pi} \int_0^1 \int_0^{2\pi} sinh^{2n}(\gamma(\rho_1+\rho_1)\, exp\left(-\gamma^2(\rho_1^2+\rho_2^2)\right) exp(ip(\epsilon_1 - \epsilon_2)) \times exp\left\{-0.0529 D^{5/3} k^2 C_n^2 z(\rho_1^{16} + \rho_2^{16} - 2\rho_1^4\rho_2^4\, cos(4\theta_1 - 4\theta_2))\right\} exp\left[i\pi\left(\frac{2b}{\lambda z}\right) r[\rho_2\, cos(\epsilon_2 - \emptyset) - \rho_1\, cos(\epsilon_1 - \emptyset)]\right] \rho_1\rho_2 d\rho_1 d\epsilon_1 d\rho_2 d\epsilon_2 \quad (27)$$

5. NUMERICAL CALCULATIONS AND DISCUSSIONS

For describing the distribution of intensity and OAM on a focused vortex ShGB that is propagated through a turbulent atmospheric environment, a numerical approach was applied for the evaluation of equations (14, 16, 20, 22, & 26) by applying the parameter values as z=f, λ is the wavelength, which is taken as1060nm, and b=0.05m. Distribution of intensity and OAM of a vortex ShGB in the presence of z-tilt, defocus, astigmatism, coma, and spherical aberration under various turbulence conditions such as zero turbulence (c_n^2=0), weak turbulence (c_n^2=0.5x$10^{-16}m^{-2/3}$), medium turbulence (c_n^2=$10^{-15}m^{-2/3}$), and strong turbulence (c_n^2=5x$10^{-15}m^{-2/3}$) with topological charge p=1 are displayed in both two dimensional (2d) and three dimensional (3d) plots.

5.1 Influence of z-tilt aberration

The influence of z-tilt aberration Fig.3(a, b, c, d) and (e, f, g, h) shows normalised three-dimensional and two-dimensional plots for the distribution of intensity at z=2000m for z-tilt aberration under four different turbulent conditions of the atmosphere such as c_n^2=0, c_n^2=0.5x$10^{-16}m^{-2/3}$, c_n^2=$10^{-15}m^{-2/3}$, and c_n^2=5x$10^{-15}m^{-2/3}$ with p=1. Fig.3(a & e) shows that the structure of generated beam is a doughnut-shaped beam with maximum OAM. The structure almost remains constant in weak turbulence also, as viewed in Fig.3(b & f) respectively. Under medium turbulence, the beam structure changes are observed, and the intensity distribution turns to be bumpy with a decrease in OAM, as shown in Fig.3(c & g). Fig.3(d & h) reveals that under strong turbulence conditions, the doughnut-shaped structure turns into almost a Gaussian beam. Thus in the presence of tilt aberration, increasing turbulence condition values will convert the doughnut-shaped focused beam into a Gaussian beam.

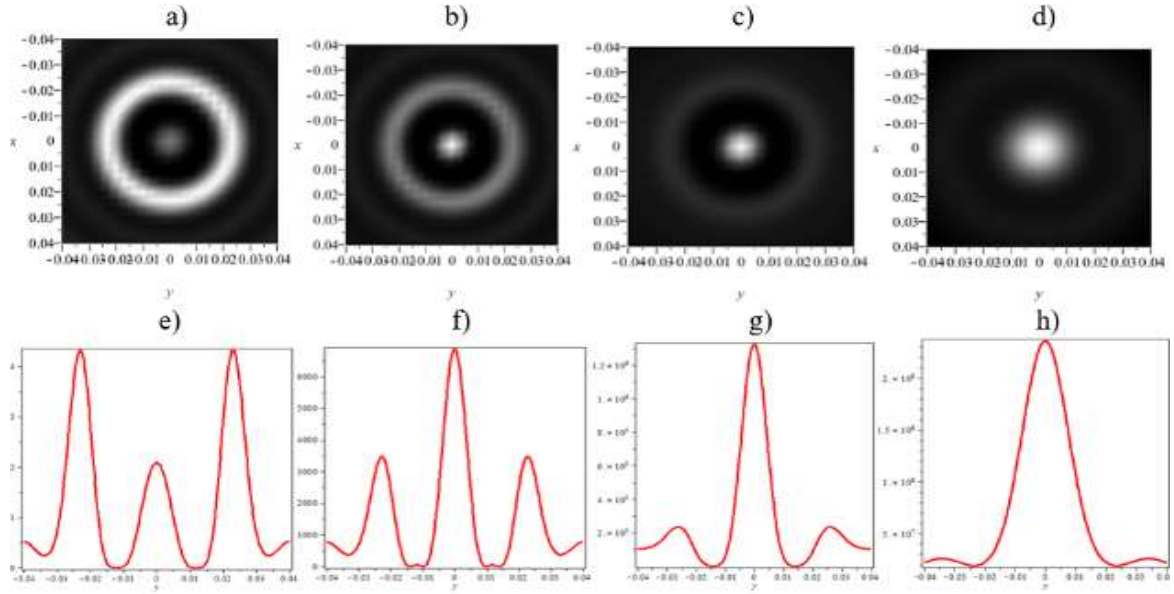

Fig.3 3d and 2d plot of the vortex ShGB of tilt aberration under (a & e) c_n^2=0, (b & f) c_n^2=0.5x$10^{-16}$$m^{-2/3}$, (c & g) c_n^2=$10^{-15}$$m^{-2/3}$, (d& h) c_n^2=5x$10^{-15}$$m^{-2/3}$ at z=2000m with p=1

Fig.4(a, b, c, d) and (e, f, g, h) shows the normalised three dimensional and two-dimensional OAM and intensity distributions at z=5000m for z-tilt aberration under four different turbulent conditions of the atmosphere such as c_n^2=0, c_n^2=0.5x10^{-16} $m^{-2/3}$, c_n^2=10^{-15} $m^{-2/3}$, and c_n^2=5x10^{-15} $m^{-2/3}$ with p=1. The figure shows that at z=5000m, the size of the doughnut structure of the beam is increased compared to z=2000m. By viewing Fig.4(a & e), we can see that the resultant intensity is ring-shaped for zero turbulence, and it is maintained under weak turbulence also with maximum OAM, which is viewed in Fig. 4(b & f), but it changes to partially Gaussian profiled beam under medium Fig.4(c & g) and complete Gaussian under strong turbulence conditions that is seen in Fig.4(d & h).

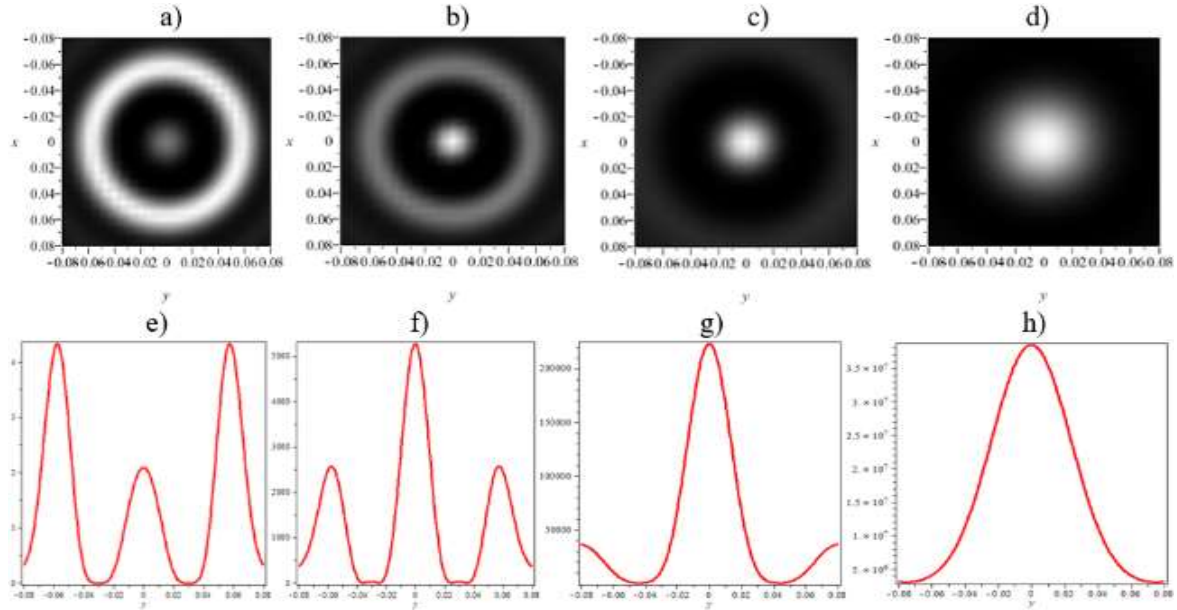

Fig. 4 3d and 2d plot of the vortex ShGB of tilt aberration under (a & e) c_n^2=0, (b & f) c_n^2=0.5x$10^{-16}$$m^{-2/3}$, (c & g) c_n^2=$10^{-15}$$m^{-2/3}$, (d& h) c_n^2=5x$10^{-15}$$m^{-2/3}$ at z=5000m with p=1

5.2 Influence of defocus aberration

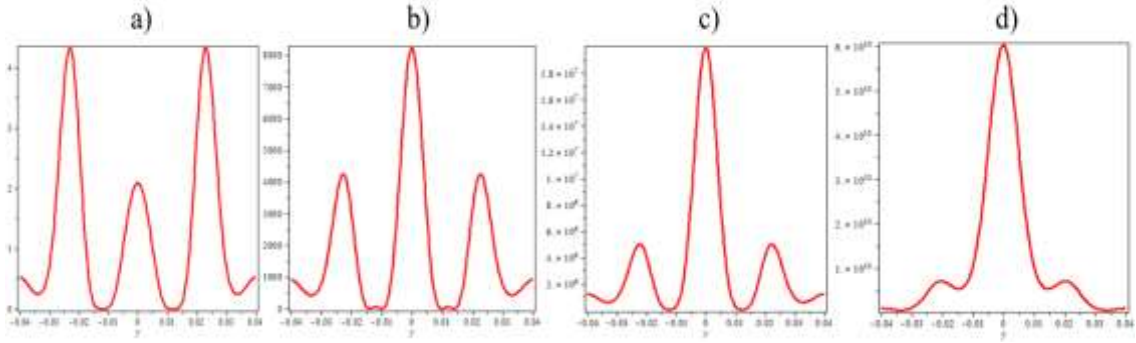

Fig.5 2D plot of the vortex ShGB of defocus aberration under (a) $c_n^2=0$, (b) $c_n^2=0.5x10^{-16}m^{-2/3}$, (c) $c_n^2=10^{-15}m^{-2/3}$, (d) $c_n^2=5x10^{-15}m^{-2/3}$ at z=2000m with p=1

Fig.5 (a, b, c, d) reveals the two dimensional distributions of ShGB intensity at z=2000m for defocus aberration under four different turbulent conditions of atmosphere such as $c_n^2=0$, $c_n^2=0.5x10^{-16}m^{-2/3}$, $c_n^2=10^{-15}m^{-2/3}$, and $c_n^2=5x10^{-15}m^{-2/3}$ with p=1. The resultant focal segment is ring-shaped with maximum OAM for $c_n^2=0$ as in Fig.5(a). OAM and doughnut structure start reducing for $c_n^2=0.5x10^{-16}m^{-2/3}$and for $c_n^2=10^{-15}m^{-2/3}$, as in Fig.5(b & c). At $c_n^2=5x10^{-15}m^{-2/3}$, the beam gets converted to Gaussian nature with very low OAM, which is shown in Fig.5(d).

Fig. 6 (a, b, c, d) reveals the two-dimensional distributions of ShGB intensity at z=5000m for defocus aberration under four different turbulent conditions of the atmosphere such as $c_n^2=0$, $c_n^2=0.5x10^{-16}m^{-2/3}$, $c_n^2=10^{-15}m^{-2/3}$, and $c_n^2=5x10^{-15}m^{-2/3}$ with p=1. The resultant focal segment is ring-shaped with maximum OAM for $c_n^2=0$ as in Fig. 6(a). OAM and doughnut structure start reducing for $c_n^2=0.5x10^{-16}m^{-2/3}$and $c_n^2=10^{-15}m^{-2/3}$, as in Fig.6(b & c), At $c_n^2=5x10^{-15}m^{-2/3}$, the beam gets converted to Gaussian nature with very low OAM, which can be viewed in Fig.6(d).

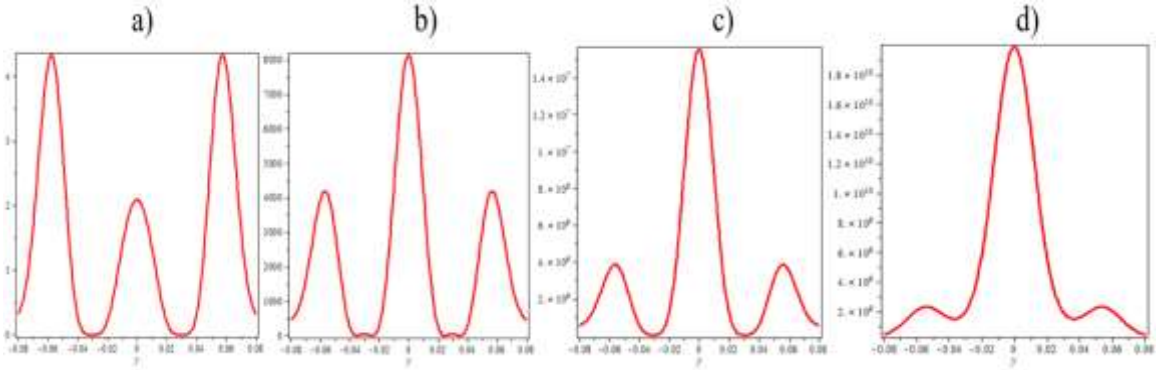

Fig. 6 2D plot of the vortex ShGB of defocus aberration under (a) $c_n^2=0$, (b) $c_n^2=0.5x10^{-16}m^{-2/3}$, (c) $c_n^2=10^{-15}m^{-2/3}$, (d) $c_n^2=5x10^{-15}m^{-2/3}$ at z=5000m with p=1

5.3 Influence of astigmatism aberration

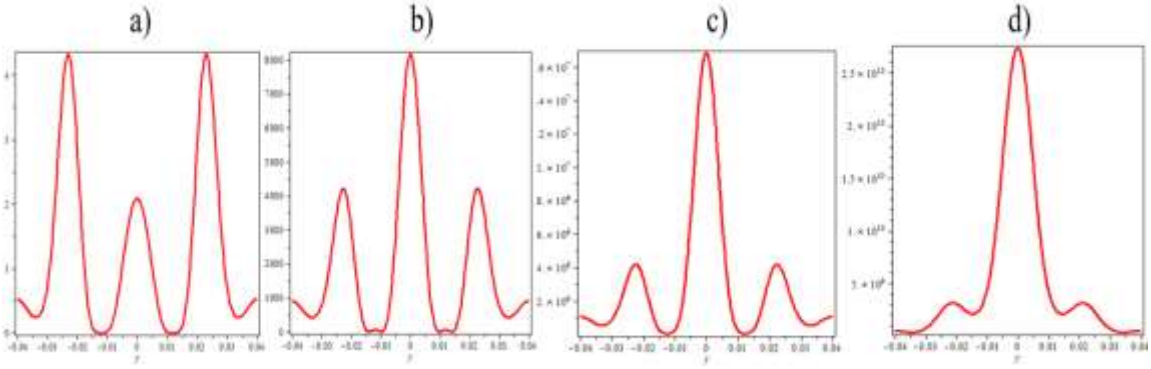

Fig. 7 2d plot of the vortex ShGB of astigmatism aberration under (a) $c_n^2=0$, (b) $c_n^2=0.5x10^{-16}m^{-2/3}$, (c) $c_n^2=10^{-15}m^{-2/3}$, (d) $c_n^2=5x10^{-15}m^{-2/3}$ at z=2000m with p=1

Fig.7(a, b, c, d) reveals the two dimensional distributions of ShGB intensity at z=2000m for astigmatism aberration under four different turbulent conditions of atmosphere such as $c_n^2=0$, $c_n^2=0.5x10^{-16}m^{-2/3}$, $c_n^2=10^{-15}m^{-2/3}$, and $c_n^2=5x10^{-15}m^{-2/3}$ with p=1. The resultant focal segment is ring-shaped with maximum OAM and intensity for $c_n^2=0$, as seen in Fig.7(a). Under weak turbulent state $c_n^2=0.5x10^{-16}m^{-2/3}$, the OAM and intensity start reducing as in Fig.7(b). Under the medium turbulent condition, i.e., $c_n^2=10^{-15}m^{-2/3,}$ the OAM and intensity again reduce, which can be viewed in Fig.7(c), and at $c_n^2=5x10^{-15}m^{-2/3}$, the beam almost takes the shape of a Gaussian beam with very low OAM, which is shown in Fig.7(d).

Fig.8(a, b, c, d) reveals the two dimensional distributions of ShGB intensity at z=5000m for astigmatism aberration under four different turbulent conditions of atmosphere such as $c_n^2=0$, $c_n^2=0.5x10^{-16}m^{-2/3}$, $c_n^2=10^{-15}m^{-2/3}$, and $c_n^2=5x10^{-15}m^{-2/3}$ with p=1. The resultant focal segment is ring-shaped with maximum OAM for $c_n^2=0$ as in Fig.8(a). OAM and doughnut structure start reducing for $c_n^2=0.5x10^{-16}m^{-2/3}$and $c_n^2=10^{-15}m^{-2/3}$, as in Fig.8(b & c). At $c_n^2=5x10^{-15}m^{-2/3}$, the beam gets converted to Gaussian nature with very low OAM, which is shown in Fig.8(d).

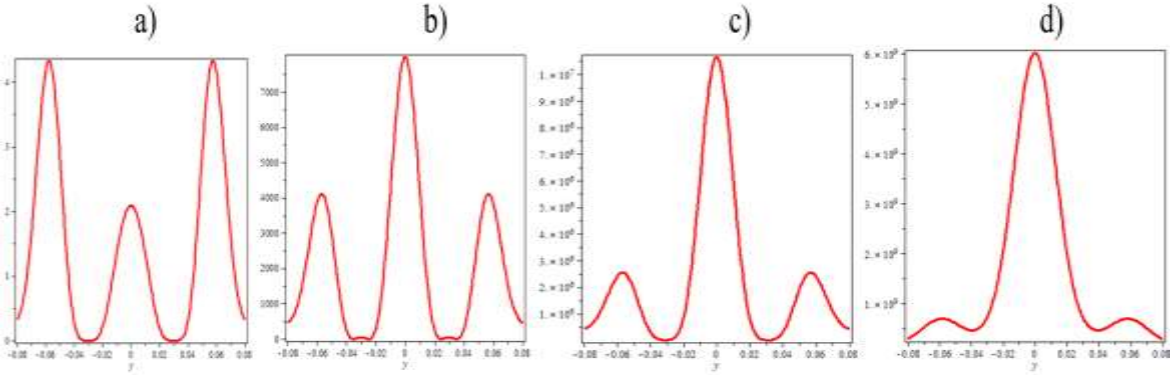

Fig. 8 2d plot of the ShGB of astigmatism aberration under (a) $c_n^2=0$, (b) $c_n^2=0.5x10^{-16}m^{-2/3}$, (c) $c_n^2=10^{-15}m^{-2/3}$, (d) $c_n^2=5x10^{-15}m^{-2/3}$ at z=5000m with p=1

5.4 Influence of coma aberration

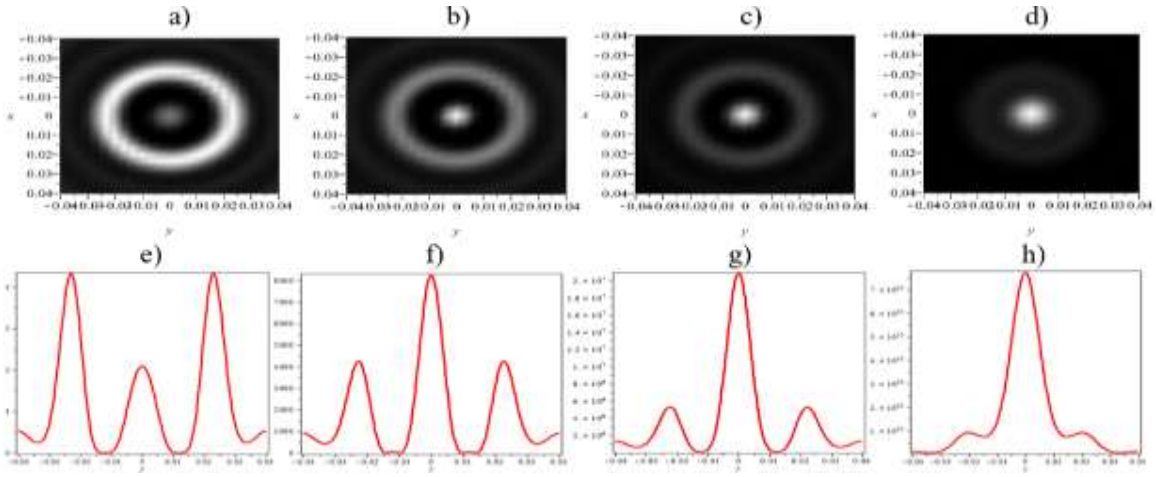

Fig. 9 3D and 2D plot of the vortex ShGB of coma aberration under (a & e) $c_n^2=0$, (b & f) $c_n^2=0.5\text{x}10^{-16}m^{-2/3}$, (c & g) $c_n^2=10^{-15}m^{-2/3}$, (d& h) $c_n^2=5\text{x}10^{-15}m^{-2/3}$ at z=2000m with p=1

Fig. 9(a, b, c, d) and (e, f, g, h) shows the normalised three and two-dimensional intensity distributions at z=2000m for coma aberration under four different turbulent conditions of the atmosphere such as $c_n^2=0$, $c_n^2=0.5\text{x}10^{-16}m^{-2/3}$, $c_n^2=10^{-15}m^{-2/3}$, and $c_n^2=5\text{x}10^{-15}m^{-2/3}$ with p=1. The resultant focal segment is ring-shaped with maximum OAM and intensity for $c_n^2=0$, as seen in Fig. 9(a & e). Under weak turbulent state $c_n^2=0.5\text{x}10^{-16}m^{-2/3}$, the OAM and intensity start reducing as in Fig. 9(b & f). Under the medium turbulent condition, i.e., $c_n^2=10^{-15}m^{-2/3}$, the OAM and intensity again reduce, which can be viewed in Fig. 9(c & g), and at $c_n^2=5\text{x}10^{-15}m^{-2/3}$, the beam almost takes the shape of a Gaussian beam with very low OAM, which can be clearly viewed in Fig. 9(d & h).

Fig. 10(a, b, c, d) and (e, f, g, h) shows the normalised three and two-dimensional intensity distributions at z=5000m for coma aberration under four different turbulent conditions of the atmosphere such as $c_n^2=0$, $c_n^2=0.5\text{x}10^{-16}m^{-2/3}$, $c_n^2=10^{-15}m^{-2/3}$, and $c_n^2=5\text{x}10^{-15}m^{-2/3}$ with p=1 at z=5000m. The resultant focal segment is ring-shaped with maximum OAM and intensity for $c_n^2=0$, as seen in Fig. 10(a & e). Under weak turbulent state $c_n^2=0.5\text{x}10^{-16}m^{-2/3}$, the OAM and intensity start reducing as in Fig. 10(b & f). Under the medium turbulent condition, i.e., $c_n^2=10^{-15}m^{-2/3}$, the OAM and intensity again reduce, which can be viewed in Fig. 10(c & g), and at $c_n^2=5\text{x}10^{-15}m^{-2/3}$, the beam almost takes the shape of a Gaussian beam with very low OAM, which can be clearly viewed in Fig. 10(d & h).

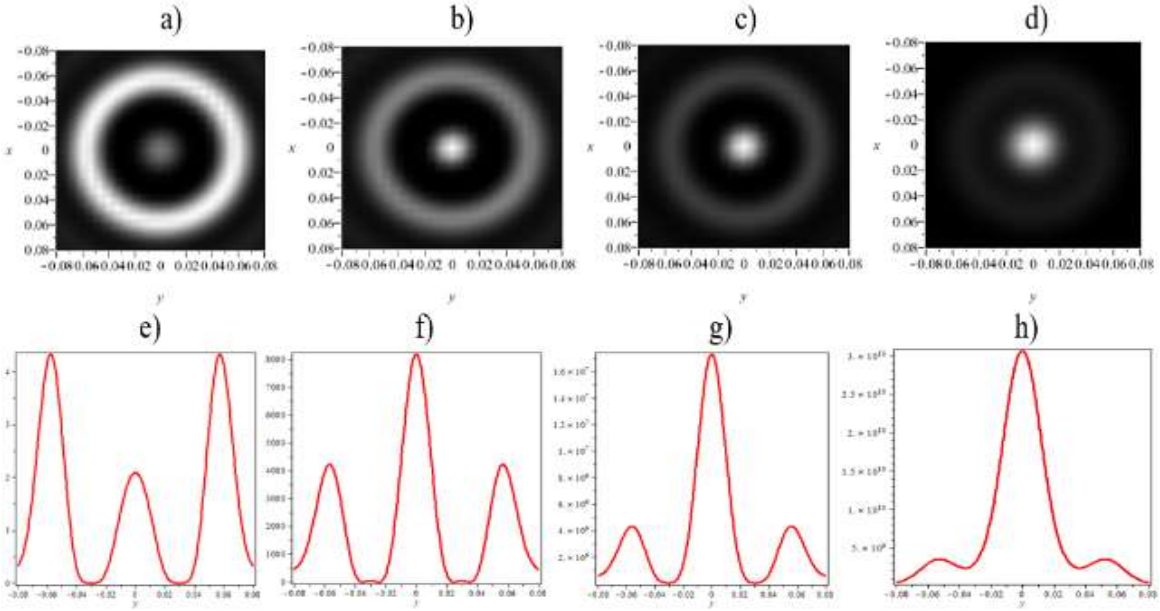

Fig. 10 3d and 2d plot of the vortex ShGB of coma aberration under (a & e) c_n^2=0, (b & f) c_n^2=0.5x10^{-16}m$^{-2/3}$, (c & g) c_n^2=10^{-15}m$^{-2/3}$, (d& h) c_n^2=5x10^{-15}m$^{-2/3}$ at z=5000m with p=1

5.5 Influence of spherical aberration

Fig. 11(a, b, c, d) reveals the two-dimensional distributions of ShGB intensity at z=2000m for spherical aberration under four different turbulent conditions of atmosphere such as c_n^2=0, c_n^2=0.5x10^{-16}m$^{-2/3}$, c_n^2=10^{-15}m$^{-2/3}$, and c_n^2=5x10^{-15}m$^{-2/3}$ with p=1. The resultant focal segment is ring-shaped with maximum OAM and intensity for c_n^2=0, as seen in Fig. 11(a). Under weak turbulent state c_n^2=0.5x10^{-16}m$^{-2/3}$, the OAM and intensity start reducing as in Fig. 11(b). Under the medium turbulent condition, i.e., c_n^2=10^{-15}m$^{-2/3,}$ the OAM and intensity again reduce, which can be viewed in Fig. 11(c), and at c_n^2=5x10^{-15}m$^{-2/3}$, the beam almost takes the shape of a Gaussian beam with very low OAM, which is shown in Fig. 11(d).

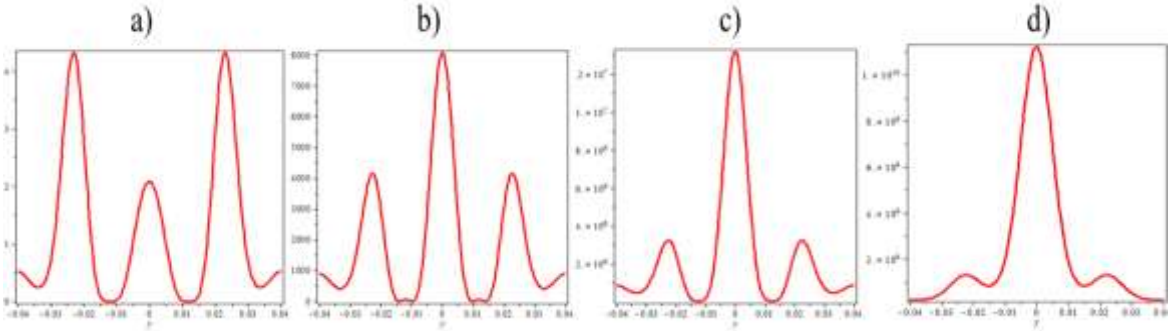

Fig. 11 2D plot of the vortex ShGB of spherical aberration under (a) c_n^2=0, (b) c_n^2=0.5x10^{-16}m$^{-2/3}$, (c) c_n^2=10^{-15}m$^{-2/3}$, (d) c_n^2=5x10^{-15}m$^{-2/3}$ at z=2000m with p=1

Fig.12 (a, b, c, d) reveals the two dimensional distributions of ShGB intensity at z=5000m for spherical aberration under four different turbulent conditions of atmosphere such as c_n^2=0, c_n^2=0.5x10^{-16}m$^{-2/3}$, c_n^2=10^{-15}m$^{-2/3}$, and c_n^2=5x10^{-15}m$^{-2/3}$ with p=1. The resultant focal segment is ring-shaped with maximum OAM and intensity for c_n^2=0, as seen in Fig.12(a). Under weak turbulent state c_n^2=0.5x10^{-16}m$^{-2/3}$, the OAM and intensity start reducing as in Fig.12(b). Under the medium turbulent condition, i.e., c_n^2=10^{-15}m$^{-2/3}$, the OAM and intensity again reduce, which

can be viewed in Fig.12(c), and at $c_n^2=5x10^{-15}m^{-2/3}$, the beam almost takes the shape of a Gaussian beam with very low OAM, which is shown in Fig.12(d).

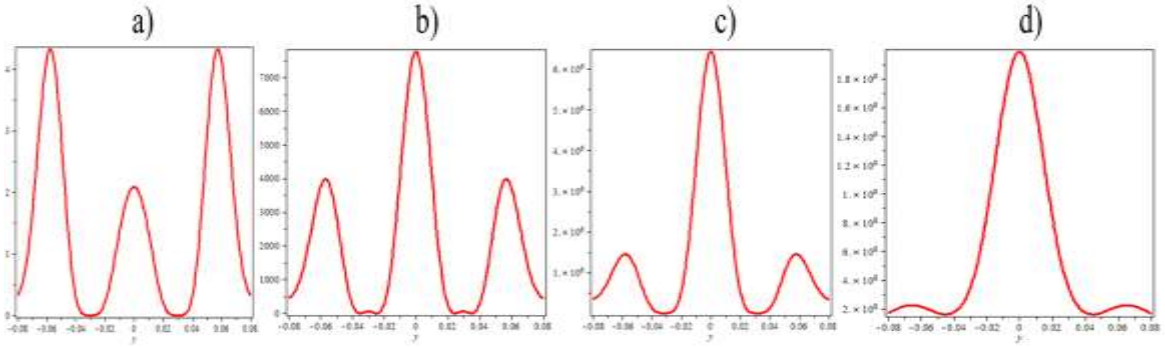

Fig. 12. 2D plot of the vortex ShGB of spherical aberration under (a) $c_n^2=0$, (b) $c_n^2=0.5x10^{-16}m^{-2/3}$, (c) $c_n^2=10^{-15}m^{-2/3}$, (d) $c_n^2=5x10^{-15}m^{-2/3}$ at z=5000m with p=1

6.COMPARISON BETWEEN THE EFFECT OF VARIOUS ABERRATIONS AT DIFFERENT TOPOLOGICAL CHARGES

The comparison analysis shows the effect of various aberrations on vortex Sinh-Gaussian beam at different topological charges z=2000m and z=5000m. Fig. 13, 14, 15, 16, and 17 shows the comparison between z-tilt, defocus, astigmatism, coma, and spherical aberration for various turbulent conditions such as $c_n^2=0$(zero turbulent condition), $c_n^2=0.5x10^{-16}m^{-2/3}$(weak turbulent condition), $c_n^2=10^{-15}m^{-2/3}$(medium turbulent condition) & $c_n^2=5x10^{-15}m^{-2/3}$ (strong turbulent condition). The red colour curve indicates the zero turbulent condition, the blue colour curve indicates a weak turbulent condition, the black colour curve indicates a medium turbulent condition, and the green colour curve indicates a strong turbulent condition. It is found that the propagation distance also plays an important role in maintaining the beam quality. As propagation distance increases, beam quality decreases.

6.1 Z-tilt aberration

Fig. 13 shows the comparison between z-tilt aberration for various turbulent conditions such as $c_n^2=0$, $c_n^2=0.5x10^{-16}m^{-2/3}$, $c_n^2=10^{-15}m^{-2/3}$, & $c_n^2=5x10^{-15}m^{-2/3}$ for p=l at z=2000m (Fig.13(a)) & z=5000 (Fig.13(b)). It is found that as the value of turbulence and propagation distance increases, tilt aberration has a high impact on the intensity distribution of vortex ShGB beam, as shown in Fig.13(a & b). At z=2000m (Fig.13(a)), we can see that the beam has maximum OAM under zero turbulence, then it is gradually decreasing when the turbulent value increases to weak, medium, and strong turbulent conditions. At medium and strong turbulence, the OAM value almost reaches zero. At z=5000m (Fig.13(b)), we can see that the beam has maximum OAM under zero turbulence, then it is gradually decreasing when the turbulent value increases to weak. Under medium and strong turbulent conditions, the OAM value is reduced to zero. Therefore, we can see that z-tilt aberration has a high impact on the OAM and intensity distribution of the beam. Also, as the turbulence conditions and propagation distance increase, it badly affects the quality of the beam.

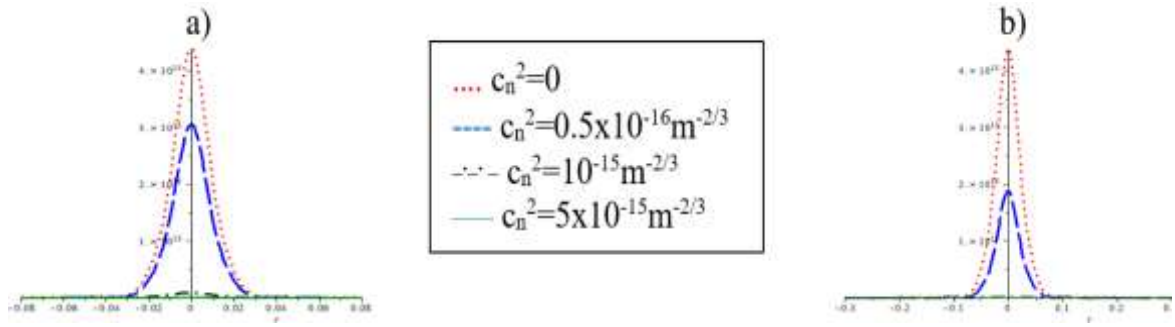

Fig. 13 Intensity profile of 2d of vortex ShGB due to z-tilt aberration in zero, weak, medium and strong turbulent conditions with p=1; for (a) z=2000m, (b) z=5000m

6.2 Defocus aberration

Fig. 14(a & b) shows the comparison between defocus aberration for various turbulent conditions such as $c_n^2=0$(zero turbulent condition), $c_n^2=0.5x10^{-16}m^{-2/3}$(weak turbulent condition), $c_n^2=10^{-15}m^{-2/3}$(medium turbulent condition), and $cn^2=5x10^{-15}m^{-2/3}$ (strong turbulent condition) for p=l at z=2000m; (Fig.14(a)) & z=5000m (Fig.14(b)). As propagation distance increases, it has high impact on intensity distribution as shown in Fig.14(b), but very less impact than tilt aberration.

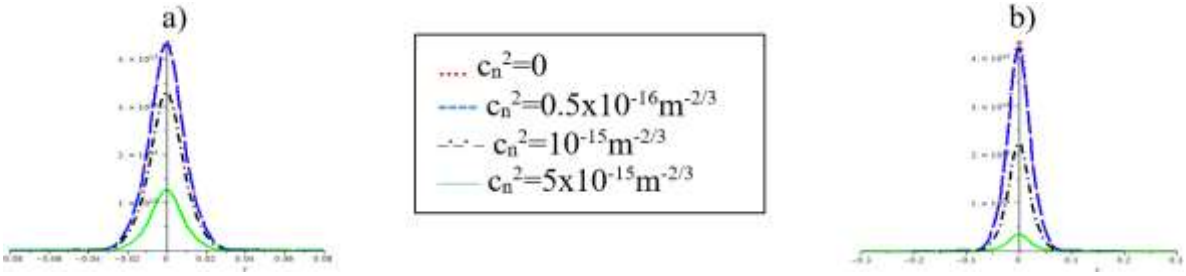

Fig. 14 Intensity profile of 2d of vortex ShGB due to defocus aberration in zero, weak, medium and strong turbulent conditions with p=1; for (a) z=2000m, (b) z=5000m

6.3 Astigmatism aberration

Fig. 15(a & b) shows the comparison between astigmatism aberration for various turbulent conditions such as $c_n^2=0$(zero turbulent condition), $c_n^2=0.5x10^{-16}m^{-2/3}$(weak turbulent condition), $c_n^2=10^{-15}m^{-2/3}$(medium turbulent condition) & $c_n^2=5x10^{-15}m^{-2/3}$ (strong turbulent condition) for p=l at z=2000m, (Fig. 15(a)) & z=5000m (Fig.15. (b)). The comparison plot shows that astigmatism has less impact on beam intensity than tilt aberration but more than defocus aberration, coma, and spherical aberrations. Also, the quality of the beam is reduced when propagation distance increases.

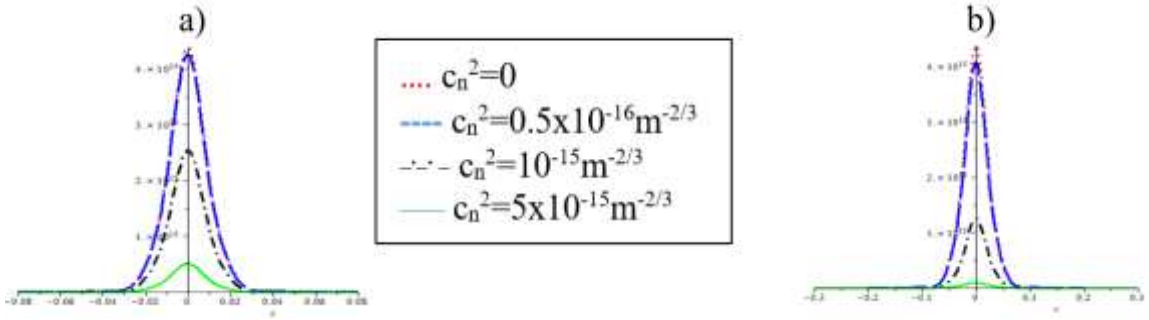

Fig. 15 Intensity profile of 2d of vortex ShGB due to astigmatism aberration in zero, weak, medium and strong turbulent conditions with p=1; for (a) z=2000m, (b) z=5000m

6.4 Coma aberration

Fig. 16 shows the comparison between coma aberration for various turbulent conditions such as c_n^2=0(zero turbulent condition), c_n^2=0.5x$10^{-16}m^{-2/3}$(weak turbulent condition), c_n^2=$10^{-15}m^{-2/3}$(medium turbulent condition) & c_n^2=5x$10^{-15}m^{-2/3}$ (strong turbulent condition) for p=l at z=2000m (Fig.16(a)) & z=5000m (Fig.16(b)). The 2d plot demonstrates that coma aberration has the least impact on the distribution of ShGB intensity with an increase in value of turbulence and propagation distance compared to all the other four aberrations.

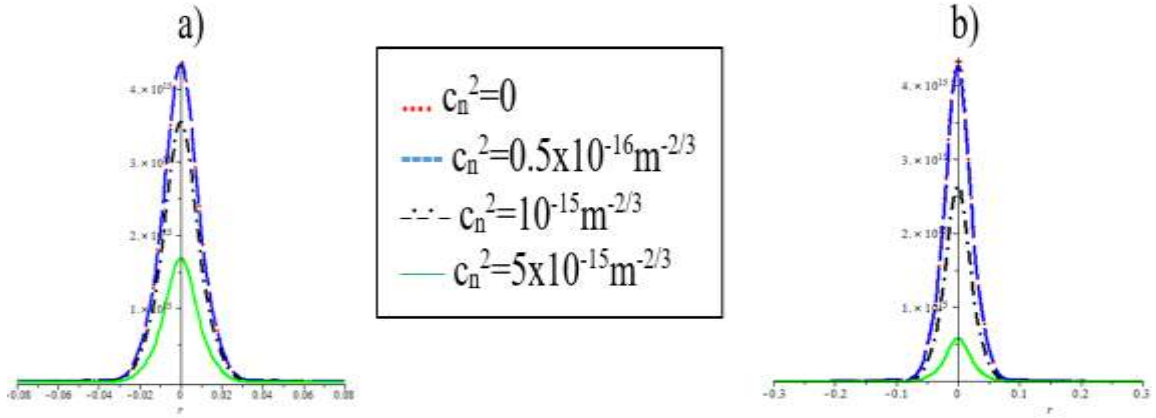

Fig. 16 Intensity profile of 2d of vortex ShGB due to coma aberration in zero, weak, medium and strong turbulent conditions with p=1; for (a) z=2000m, (b) z=5000m

6.5 Spherical aberration

Fig. 17 shows the comparison between spherical aberration for various turbulent conditions such as c_n^2=0(zero turbulent condition), c_n^2=0.5x$10^{-16}m^{-2/3}$(weak turbulent condition), c_n^2=$10^{-15}m^{-2/3}$(medium turbulent condition) & c_n^2=5x$10^{-15}m^{-2/3}$ (strong turbulent condition) for p=l at z=2000m (Fig.17(a)) & z=5000m (Fig.17. (b)). The results reveal that the influence of spherical aberration on the intensity distribution of beam is less than tilt and astigmatism but more than defocus and coma aberrations. Also, the quality of the beam reduces with an increase in propagation distance.

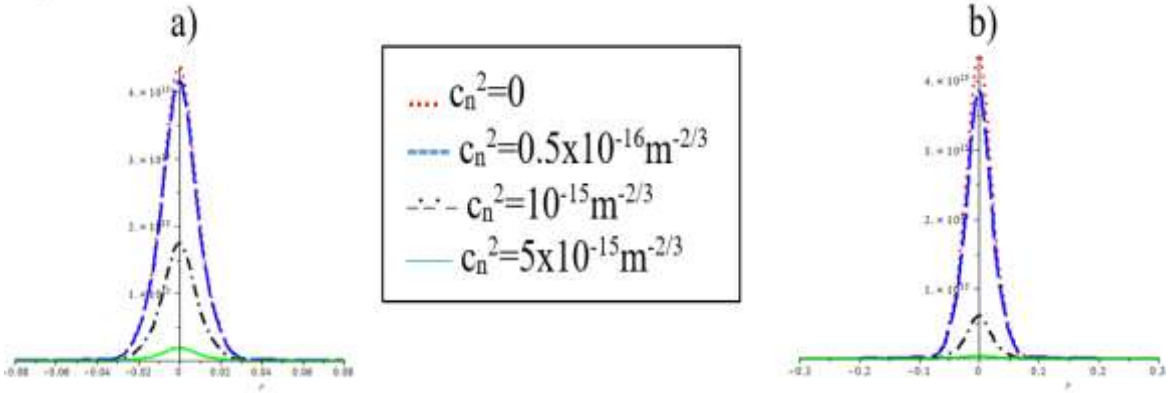

Fig. 17. Intensity profile of 2d of vortex ShGB due to spherical aberration in zero, weak, medium and strong turbulent conditions with p=1; for (a) z=2000m, (b) z=5000m

7.CONCLUSION

Here, we have investigated the change in OAM and intensity distribution of vortex ShGB beam, which has been affected by z-tilt, defocus, astigmatism, coma, and spherical aberration

using the Fresnel-Kirchhoff diffraction integral principle under various atmospheric turbulent conditions such as zero, weak, medium, and strong atmospheric turbulent conditions with topological charge p=1 at various propagation distance z=2000m and z=5000m. For each aberration, numerical analysis was performed, and both 2d and 3d plots were plotted. The analysis shows that z-tilt aberration has the highest impact on affecting OAM and intensity distribution of the ShGB compared to all the other four aberrations. Results reveal that due to the influence of tilt aberration, the OAM and intensity distribution of vortex ShGB decays with an increase in value of the structural constant of atmospheric turbulence. Also, when we increase the propagation distance from z=2000m to 5000m, again, it shows the quality of the beam is reduced badly. The overall comparison reveals that z-tilt aberration has a severe influence on the OAM and intensity distribution of vortex ShGB. Coma aberration has the least influence on OAM and distribution of intensity on vortex ShGB beam.

DECLARATIONS

Funding: There is no funding provided to prepare the manuscript.

Conflict of Interest: There is no conflict of Interest between the authors regarding the manuscript preparation and submission.

Ethical Approval*:* This article does not contain any studies with human participants or animals performed by any of the authors.

Informal Consent**:** Informed consent was obtained from all individual participants included in the study.

Consent to participate**:** I have read and I understand the provided information.

Consent to Publish**:** This article does not contain any Image or video to get permission.

Data availability statement: If all data, models, and code generated or used during the study appear in the submitted article and no data needs to be specifically requested.

Code availability: No code is available for this manuscript.

REFERENCES

1. G. Zhao, and Y. Zhang, The effect of tilt aberration and astigmatism of turbulent atmosphere on the intensity distribution of a vortex carrying Gaussian beam. Optik, 122(1), 29-32 (2011). https://doi.org/10.1016/j.ijleo.2009.05.033.

[2]Y.A. Teen, P.Suresh, T. Nathiyaa, K.B. Rajesh and T.V.S. Pillai, Study on intensity distributions of a BG beam with effect of tilt and astigmatism aberration in a turbulent atmosphere. Optik, 126(23), 3830-3837 (2015). https://doi.org/10.1016/j.ijleo.2015.07.137.

[3]R. K., Singh, P. Senthilkumaran, and K. Singh, Focusing of a vortex carrying beam with Gaussian background by an apertured system in presence of coma. Optics communications, 281(5), 923-934 (2008). https://doi.org/10.1016/j.optcom.2007.10.070.

[4]R. K. Singh, P. Senthilkumaran and K. Singh, Focusing of a singular beam in the presence of spherical aberration and defocusing. Optik, 119(10), 459-464 (2008). https://doi.org/10.1016/j.ijleo.2006.11.012.

[5]G. Zhao, and Y. Zhang The effect of tilt aberration and astigmatism of turbulent atmosphere on the intensity distribution of a vortex carrying Gaussian beam. Optik, 122(1), 29-32 (2011). https://doi.org/10.1016/j.ijleo.2009.05.033.

[6]T. Wang, J.Pu, and Z. Chen, Beam-spreading and topological charge of vortex beams propagating in a turbulent atmosphere. Optics Communications, 282(7), 1255-1259 (2009) .https://doi.org/10.1016/j.optcom.2008.12.027.

[7]J. Lin, Y. Ma, P. Jin, G. Davies and J. Tan, Longitudinal polarized focusing of radially polarized sinh-Gaussian beam. Optics Express, 21(11), 13193-13198. (2013) https://doi.org/10.1364/oe.21.013193.

[8]C. M. Sundaram, K.Prabakaran, P.M. Anbarasan, K.B. Rajesh, A.M. Musthafa and V. Aroulmoji, Tight focusing properties of phase modulated transversely polarized sinh Gaussian beam. Optical and Quantum Electronics, 49(1), 1-10 (2017). https://doi.org/10.1007/s11082-016-0857-7.

[9]Y.Zhang, X. Zho uand X. Yuan, Performance analysis of sinh-Gaussian vortex beams propagation in turbulent atmosphere. Optics Communications, 440, 100-105 (2019). https:// doi.org/10.1016/j.optcom.2019.02.007.

[10]Z. Liu, X.Wang and K.Hang, Enhancement of trapping efficiency by utilizing a hollow sinh-Gaussian beam. Scientific Reports, 9(1), 1-8 (2019). https://doi.org/10.1038/s41598-019-46716-5.

[11]A.A. Kovalev, V.V. Kotlyar, and A.P. Porfirev, Orbital angular momentum and topological charge of a multi-vortex Gaussian beam. JOSA A, 37(11) 1740-1747 (2020). https://doi.org/10.1364/JOSAA.401561.

[12]Z. Hricha, M.Yaalou, & A. Belafhal, Propagation of hollow sinh-Gaussian beams in strongly nonlocal nonlinear media. Optics Communications, 478, 126400. (2021) https://doi.org/10.1016/j.optcom.2020.126400.

[13]Z. Liu, X.Wang, and K. Hang, Enhancement of trapping efficiency by utilizing a hollow sinh-Gaussian beam. Scientific Reports, 9(1), 1-8 (2019). https://doi.org/10.1038/s41598-019-46716-5.

[14]J. Wang, Advances in communications using optical vortices. Photonics Research, 4(5), B14-B28 (2016). https://doi.orgt/10.1364/prj.4.000b14.

[15]L. Zhao, T.Jiang, M.Mao, Y.Zhang, H.Liu, Z.Wei,... A. Luo, Improve the capacity of data transmission in orbital angular momentum multiplexing by adjusting link structure. IEEE Photonics Journal, 12(3) 1-11 (2014). https://doi.orgt/10.1109/jphot.2020.2985728.

[16]X. Wang, Z.Liu, and D. Zhao, Fractional Fourier transform of hollow sinh-Gaussian beams. Optical Engineering, 53(8) 086112 (2014) . https://doi.org/10.1117/1.oe.53.8.086112.

[17]Q. Sun, K.Zhou, G.Fang, G.Zhang, Z.Liu, & S. Liu, Hollow sinh-Gaussian beams and their paraxial properties. Optics Express, 20(9) (2012) 9682-9691. https://doi.org/10.1364/oe.20.009682.

[18]K. Zhu, R.Liang, Y.Yi, J.Zhu and H. Tang, Propagation invariance and dark hollow structures of sinh-Gaussian beams with small complex parameters. In Journal of Physics: Conference Series 1732(1), 012163 (2021). IOP Publishing. https://doi.org/10.1088/1742-6596/1732/1/012163.

[19]R. J. Noll, Zernike polynomials and atmospheric turbulence. JOSA, 66(3) 207-211(1976). https://doi.org/10.1364/josa.66.000207.

[20]P.H. Hu, J.Stone and T. Stanley, Application of Zernike polynomials to atmospheric propagation problems. JOSA A, 6(10) 1595-1608 (1989). https://doi.org/10.1364/josaa.6.001595.
[21]L. C. Andrews and R.L.Phillips, Laser Beam Propagation through Random Media, Second edition, SPIE press-The International Society for Optical Engineering, Bellingham, Washington USA, 2005.
[22]G.A. Reider, Photonics – An Introduction, Springer, ISBN 978-3-319-26074-7 ISBN 978-3-319-26076-1.
[23]H. J. Eichler and J.E.O. Lux, Lasers Basics, Advances, and Applications, Springer.